PAPER

Check for updates

Quantitative elemental analysis of human leukemia K562 single cells by inductively coupled plasma mass spectrometry in combination with a microdroplet generator†

Yu-ki Tanaka, [ID] * Hinano Katayama, Risako Iida and Yasumitsu Ogra [ID]

Single-cell inductively coupled plasma mass spectrometry (scICP-MS) is an emerging technique for the determination of elemental contents in individual cells. No standardized system for the introduction of cultured mammalian cells has been established owing to difficulties in cell transport and detection. The transport efficiency of human chronic myelogenous leukemia K562 cells (hereinafter "K562 cells") in a conventional sample introduction system comprising a pneumatic nebulizer and a total consumption spray chamber is low owing to cell damage. To improve cell transport efficiency, we installed a piezo-actuator-driven microdroplet generator (μDG) into the sample introduction system of an ICP-MS for fast time-resolved analysis. Cell transport efficiency was drastically improved by using a μDG. For the determination of elemental contents, calibration curves were created by analyzing microdroplets of ionic standard solutions generated by the μDG. The pulsed signals originating from the microdroplets were analyzed and the sensitivity (*i.e.*, signal intensity per elemental mass) was calculated for each element. The quantification protocol was validated using silver nanoparticles, titanium dioxide nanoparticles, and dried yeast cells. Finally, we introduced intact K562 cells and detected signals with high throughput. The average masses of five essential elements in single K562 cells were precisely determined as follows: 270 ± 100 fg for Mg, 23.0 ± 2.0 fg for Zn, 7684 ± 675 fg for P, 2136 ± 165 fg for S, and 14.4 ± 1.2 fg for Fe. These values are consistent with the values obtained by solution nebulization ICP-MS analysis after the acid digestion of K562 cells.

Introduction

Fast time-resolved analysis by inductively coupled plasma mass spectrometry (ICP-MS) has been used to determine elemental contents in single nanoparticles. Recently, we have witnessed the application of this analytical technique to single cells as well. Trace elements in a single cell can be detected as transient signals by fast time-resolved analysis by ICP-MS with data acquisition periods shorter than 1 ms. In elemental analysis by single-cell ICP-MS (scICP-MS), living cells originating from bacteria,[1–4] fungi,[5–9] plants,[9–13] mastigophorans,[14] and mammals[9,15–28] have been used to quantify endogenous and exogenous elements in the cells. Conventional single-cell analysis based on fluorescence intensity[29,30] and cell sorting technologies[31] can be combined with elemental analysis by scICP-MS to further extend the applications of the latter in medical and biological fields.

In scICP-MS analysis, a cell suspension is directly introduced into ICP by using a conventional pneumatic nebulizer and a total consumption spray chamber at a low sample flow rate. In our previous research, the transport efficiencies of yeast, green alga, and red blood cells in ICP-MS were approximately 10%.[9] When a concentric nebulizer with a capillary tube was applied, the transport efficiency of yeast cell sample was markedly improved to higher than 70%.[5] Microfluidic devices, Dean flow-based focusing systems, and negative magnetophoresis focusing systems were used prior to the nebulizer for efficient cell transport at a constant rate.[15,24–27] Despite the development of high-throughput sample introduction devices, there is still no standardized sample introduction system for cultured mammalian cells. In the case of mammalian cells, cell damage as a result of nebulization may occur without chemical fixation, hindering access to reliable elemental data. Chemical fixation enhances the mechanical strength of mammalian cells, enabling the efficient detection of pulsed signals from the cells.[16,17,28] However, the contents of intracellular elements, especially free ions, may be altered by chemical fixation. Although transport efficiency is affected by both cell damage and loss during transportation reaching to ICP, great care must

Graduate School of Pharmaceutical Sciences, Chiba University, 1-8-1 Inohana, Chuo, Chiba 260-8675, Japan. E-mail: yu-ki.tanaka@chiba-u.jp; Fax: +81 43 226 2945; Tel: +81 43 226 2945

216 | *J. Anal. At. Spectrom.*, 2025, **40**, 216–225

This journal is © The Royal Society of Chemistry 2025

be taken for cell damage of mammalian cells which seem to be more fragile than the other types of cells. Therefore, a sample introduction system that can avoid damage to unfixed cells is desired.

To minimize damage caused by nebulization to the unfixed cells, droplet dispensers that can gently produce microdroplets in a constant cycle have been employed.[32–34] Among these, the piezo-electric microdroplet generator (μDG) is the most widely used in the sample introduction system of a scICP-MS. Although the volume of solvent introduced into ICP is reduced by using μDG, the size of droplets is larger than that of droplets from the nebulizer. Concentric helium (He) flow is typically introduced as the desolvation gas to achieve a high ionization efficiency of elements in the droplets.[34–36] Kocic et al. revealed that elements were detected with high sensitivity by adding nitrogen as the desolvation gas under the use of a high-sensitivity sampler cone.[37] The use of a heating device[17,34] and a membrane desolvator[32] prior to ionization by ICP also contributes to the efficient removal of water molecules from the ejected droplets. Rosenkranz et al. developed a μDG-based sample introduction system in combination with a conventional pneumatic nebulizer and spray chamber with impact bead for the precise determination of elemental contents in nanoparticles based on the signals of nebulized ionic standard solution.[36] Although μDG was adopted for the measurement of nanoparticles[35,37] and yeast cells,[33] few studies have used μDG for the analysis of cultured mammalian cells.[34] Unlike pneumatic nebulizers, μDG is expected to introduce cell samples without critically damaging cells. In this study, we installed a μDG into a sample introduction system of cultured mammalian cells to achieve efficient and quantitative elemental analysis at the single-cell level.

Experimental

Reagents

Ionic standard solutions of silicon (Si), silver (Ag), titanium (Ti), magnesium (Mg), zinc (Zn), sulfur (S), and iron (Fe) were purchased from Kanto Chemical (Tokyo, Japan), and ionic standard solution of phosphorus (P) was purchased from FUJIFILM Wako Pure Chemicals (Osaka, Japan). Silica (SiO$_2$; i.d. 200 nm, density (ρ) = 2.63 g cm^{-3}), Ag (i.d. 60 nm, i.d. 100 nm, ρ = 10.49 g cm^{-3}), and titanium oxide (TiO$_2$; i.d. 300 nm, ρ = 2.2 g cm^{-3}) nanoparticles were purchased from Sigma Aldrich (Saint Louis, MO, USA). SiO$_2$ microparticles (i.d. 10 μm, i.d. 20 μm, ρ = 1.8–2.0 g cm^{-3}) were purchased from microParticles GmbH (Berlin, Germany). Milli-Q water with a specific resistance of 18.2 MΩ cm (Merck Millipore, Burlington, MA, USA) was used throughout the study.

Cell samples

Commercially available dried yeast (Saccharomyces cerevisiae) was purchased from Sala Akita Shirakami Corporation (Akita, Japan). Approximately 0.02 g of yeast was suspended in Milli-Q water and washed three times by centrifugation at 10 000×g for 5 min. Human chronic myelogenous leukemia (K562) cells were

obtained from the RIKEN BRC through the National Bio-Resource Project of the MEXT/AMED, Japan (RCB0027, Tsukuba, Japan). K562 cells were cultured in RPMI-1640 (Sigma-Aldrich) supplemented with 10% fetal bovine serum (FBS; Biosera, Nuaille, France) and penicillin (100 U mL^{-1})–streptomycin (100 μg mL^{-1}) mixture (FUJIFILM Wako Pure Chemicals). For scICP-MS analysis, the cells were washed with and suspended in 0.9% high-purity sodium chloride solution (99.999%, Sigma-Aldrich). The cell density in the suspension was determined by direct microscopic count using a Bürker–Türk-type hemocytometer.

Sample introduction system for fast time-resolved ICP-MS analysis

We analyzed particle and cell samples using two sample introduction systems. (i) For the conventional single-particle (sp)ICP-MS and scICP-MS analyses, a concentric glass nebulizer (MicroMist, Glass Expansion, Victoria, Australia) and a total consumption spray chamber (Single-Cell Sample Introduction System for Agilent ICP-MS, Glass Expansion) were employed in combination with a micro syringe pump (MSP-1D, AS ONE, Osaka, Japan). (ii) For droplet analysis, a μDG (IJHB30, IJHB100, or IJHB300, MICROJET, Nagano, Japan) was inserted into the MicroJet gas adapter located at one end of the fabricated T-shaped glass plumbing, and the other ends of the glass plumbing were fit to the total consumption spray chamber and the ICP torch (Fig. 1). Inner diameters of the tip of nozzle for each μDG were 25, 40, and 60 μm, respectively. The MicroJet gas adapter, which is used in the total consumption spray chamber as an attachment, can introduce sheath gas even when used together with the μDG. We used He as the sheath gas for efficient desolvation of the solvent of the droplets. The droplets were transported approximately 15 cm in the vertical direction and further into the ICP with the aid of horizontal argon (Ar) flow. Here, no heating device or membrane desolvator was adopted. To confirm whether the elements in the droplets were completely ionized by ICP in the absence of a heating device or a membrane desolvator, we evaluated the linearity of the signals obtained from differently sized droplets from the same ionic solution (Mg: 2 μg mL^{-1}, Zn: 0.1 μg mL^{-1}, P: 30 μg mL^{-1}, S: 10 μg mL^{-1}, Fe: 0.4 μg mL^{-1}). Droplet size was determined by a CCD camera with a high-speed stroboscopy system. As illustrated in Fig. 1, we affixed the total consumption spray chamber to the T-shaped glass plumbing following the report of Rosenkranz et al.[36] The standard solution for each analyte (Ag: 0.01 μg mL^{-1}, Ti: 0.01 μg mL^{-1}, Mg: 0.05 μg mL^{-1}, Zn: 0.01 μg mL^{-1}, P: 0.5 μg mL^{-1}, S: 0.2 μg mL^{-1}, Fe: 0.01 μg mL^{-1}) was introduced into the nebulizer at a flow rate of 15 μL min^{-1} before and after the analysis of droplet samples. The signal of ions in the standard solution was used for the calibration of instrumental sensitivity drift. To evaluate whether the signal intensities of the standard solutions can correct the changes in instrumental sensitivity, we intentionally defocused the ICP-MS parameters (i.e., RF power and deflect voltage) once optimized during tuning and Mg, Zn, P, S, and Fe signals from droplet samples were applied to the correction. RF power was set to 1400, 1500,

This journal is © The Royal Society of Chemistry 2025

J. Anal. At. Spectrom., 2025, **40**, 216–225 | 217

and 1600 W, and deflect voltage was set to 5.0, 7.5, 10.0, 12.5, and 15.0 V, respectively.

The sample introduction system established here was attached to an ICP-MS/MS in the fast time-resolved analysis mode (Agilent 8900 ICP-MS/MS, Agilent Technologies, Hachioji, Japan). All calculations were carried out by ICP-MS MassHunter software (Agilent Technologies). Details of instrumentation and operational settings for ICP-MS analysis are listed in Table 1.

Determination of elemental contents by solution nebulization ICP-MS

To determine the elemental contents in a single K562 cell, the elemental contents in a cell pellet were measured by solution nebulization ICP-MS after acid digestion. Concentrated nitric acid (60%, FUJIFILM Wako Pure Chemicals) was added to the cell pellet, and cell-containing nitric acid was transferred to a PFA vial and heated in a microwave oven. After acid digestion, the sample was diluted with Milli-Q water and subjected to solution nebulization ICP-MS analysis. Mg, Zn, P, S, and Fe contents were determined by the standard addition method using an ICP-MS/MS (Agilent 8800 ICP-MS/MS, Agilent Technologies). To confirm the influence of chemical fixation on elemental contents, K562 cells were fixed with cold 70% methanol (FUJIFILM Wako Pure Chemicals) and washed with Milli-Q water three times. Then, the fixed cells were acid-digested and used for solution nebulization ICP-MS analysis. We also measured the elemental contents in a single yeast cell after the acid digestion. For both K562 and yeast cells, the elemental contents per single cell level were calculated by dividing the total mass of the elements by the number of cells subjected to acid digestion. The elemental contents in the nanoparticles were calculated from the particle radius, density, and mass fraction provided by the manufacturers.

Table 1 Instrumentation and operational settings

1. Solution nebulization ICP-MS

Instrument	Agilent 8800 ICP-MS/MS
ICP incident power	1550 W
Ar carrier gas	1.0 L min^{-1}
Integration time	100 ms
Collision/reaction cell	Disabled (Mg, Zn)
	O$_2$: 0.38 mL min^{-1} (P, S)
	H$_2$: 5.5 mL min^{-1} (Fe)

2. Single-particle/cell ICP-MS

Instrument (ICP-MS)	Agilent 8900 ICP-MS/MS
ICP incident power	1600 W
Ar carrier gas	0.60–0.65 L min^{-1}
Make-up gas (Ar)	0.15–0.20 L min^{-1}
Desolvation gas (He)	0.20 L min^{-1}
Integration time	0.1 ms
Collision/reaction cell	Disabled (Ag, Mg, Zn)
	O$_2$: 0.38 mL min^{-1} (Ti, P, S)
	H$_2$: 5.5 mL min^{-1} (Fe, Si)
Instrument (µDG)	IJHB30, 100, 300

	IJHB30	IJHB100	IJHB300
Applied voltage	36–38 V	26 V	28 V
Ejection frequency	120 Hz	120 Hz	200 Hz
1st pulse duration	120 µs	85–86 µs	80 µs
Pause duration	26–27 µs	40 µs	32 µs
2nd pulse duration	30 µs	30 µs	30 µs

Evaluation of transport efficiencies of particles and cells in conventional sp/scICP-MS

To evaluate the transport efficiencies of particles and cells in the conventional sample introduction system for sp/scICP-MS, SiO$_2$ particles with different sizes (200 nm, 10 µm, and 20 µm in
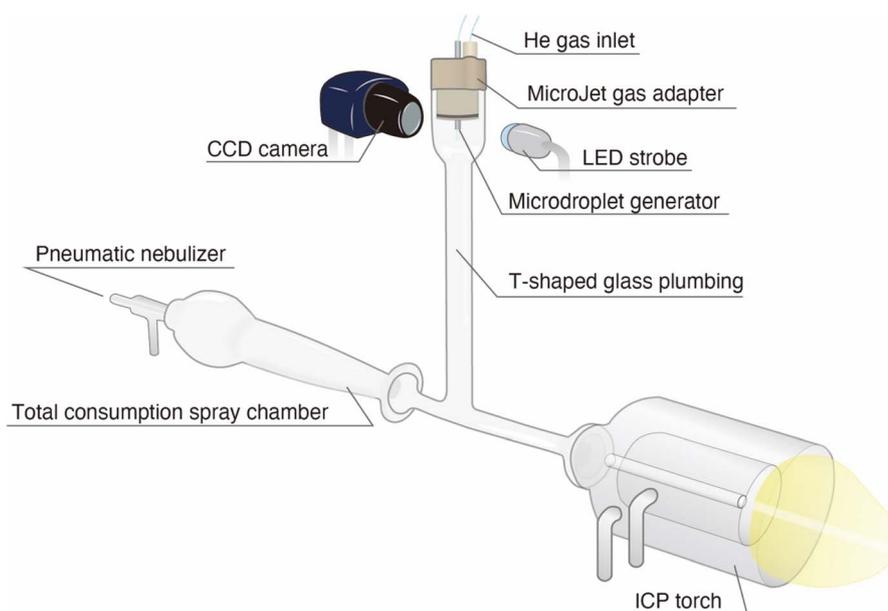

Fig. 1 Configuration of the sample introduction system with µDG.

218 | J. Anal. At. Spectrom., 2025, **40**, 216–225

This journal is © The Royal Society of Chemistry 2025

diameter), yeast cells, and K562 cells introduced with the concentric glass nebulizer and the total consumption spray chamber were analyzed. The SiO$_2$ particles were suspended in Milli-Q water at 1.8–2.4 × 10^5 mL^{-1}, yeast cells were suspended in Milli-Q water at 1.0 × 10^6 mL^{-1}, and K562 cells were suspended in 0.9% NaCl solution at 6.5 × 10^6 mL^{-1}. The suspensions were introduced into an ICP-MS at the flow rate of 15 µL min^{-1} using the micro syringe pump. We monitored the ^{28}Si signal in the H$_2$-collision mode for the SiO$_2$ particles and the ^{31}P^{16}O signal in the O$_2$-mass shift mode for the yeast cells and the K562 cells by using a fast time-resolved ICP-MS (Agilent 8900 ICP-MS/MS). The number of transient signals within a signal monitoring period of 40 s was counted. Then, the transport efficiency was calculated as the ratio of the number of transient signals to the number of particles/cells introduced into the ICP-MS for 40 s.

Microscopy observation of K562 cells after nebulization

To examine the influence of nebulization on K562 cell structure, we collected K562 cells nebulized from a MicroMist nebulizer under the Ar carrier gas flow rates of 0, 0.2, 0.4, and 0.6 L min^{-1}. The atomized aerosols including cells were directly collected by condensation on the wall of plastic tube. The collected cell samples were divided into two vials and stained with a far-red fluorescent DNA dye (1:500, DRAQ5™, BioStatus, Leicestershire, UK) or crystal violet (FUJIFILM Wako Pure Chemicals). Then, the cells were observed under a fluorescence phase-contrast microscope (BZ-X810, Keyence, Osaka, Japan). For comparison, K562 cells ejected from a µDG (IJHB300) were also observed in the same manner as the nebulized cells.

Measurements of single nanoparticles and living cells by µDG-ICP-MS

Droplets of ionic standard solutions were analyzed by fast time-resolved ICP-MS (Agilent 8900 ICP-MS/MS). The concentrations of elements in the standard solutions were as follows: Ag: 0.1 µg mL^{-1} (Ag nanoparticles); Ti: 0.1 µg mL^{-1} (TiO$_2$ nanoparticle); Mg: 0.05, 0.25 µg mL^{-1}; Zn: 0.002, 0.05 µg mL^{-1}; P: 2.5, 5.0 µg mL^{-1}; S: 0.4, 1.0 µg mL^{-1}; and Fe: 0.002, 0.05 µg mL^{-1} (yeast); Mg: 0.4, 2.0, 4.0 µg mL^{-1}; Zn: 0.25, 1.25, 2.5 µg mL^{-1}; P: 20, 100, 200 µg mL^{-1}; S: 12.5, 62.5, 125 µg mL^{-1}; and Fe: 0.25, 1.25, 2.5 µg mL^{-1} (K562). The signal intensities of ^{107}Ag, ^{48}Ti^{16}O, ^{26}Mg, ^{66}Zn, ^{31}P^{16}O, ^{32}S^{16}O, and ^{56}Fe were monitored. The mass of each element in a single droplet was calculated on the basis of droplet radius (r) and the concentration of the element in the standard solution (C). The sensitivity factor (f, cps fg^{-1}), defined as signal intensity (I_{std}) over mass, was obtained for each analyte element (eqn (1)).

$$f = \frac{I_{std}}{\frac{4}{3}\pi r^3 \times C} \quad (1)$$

Then, microdroplets containing Ag and TiO$_2$ nanoparticles, yeast cells suspended in Milli-Q, and K562 cells suspended in 0.9% NaCl solution were generated by the µDG (IJHB30 for

nanoparticles, IJHB100 for yeast, and IJHB300 for K562 cells, respectively). The particle density was adjusted to 1.7 × 10^6 mL^{-1} for 60 nm Ag, 5.5 × 10^6 mL^{-1} for 100 nm Ag, and 3.2 × 10^7 mL^{-1} for 300 nm TiO$_2$. The cell density was adjusted to 5.2 × 10^6 cells mL^{-1} for yeast and 1.0 × 10^5 cells mL^{-1} for K562 cells. Pulsed signals originating from the nanoparticles or cells were detected at a dwell time of 0.1 ms. Finally, the signal intensity (I_{smp}) was converted into mass (m) using the sensitivity factor f (eqn (2)).

$$m = \frac{I_{smp}}{f} \quad (2)$$

For the cell samples, multiple standard solutions were measured to obtain the slopes of the calibration curves (i.e., sensitivity factor f). Moreover, I_{smp} was determined by subtracting the y-intercept of the calibration curve from the signal intensity of the cell sample before calculation following eqn (2). The number of transient signals within a signal monitoring period (20 s for 60 nm Ag, 300 nm TiO$_2$, and yeast cells; 60 s for 100 nm Ag; 500 s for K562 cells) was counted. Then, transport efficiency was calculated as the ratio of the number of transient signals to the number of particles/cells introduced into the ICP-MS during each signal monitoring period. Long-term stability of transport efficiency was evaluated over 4 h using TiO$_2$ nanoparticles with the µDG (IJHB30).

The inner diameter of the µDG nozzle is typically smaller than the sample inlet of a pneumatic nebulizer. To avoid the clogging of cell samples at the tip of µDG, we continued ejection of droplets even at the interval of analysis. In addition, when the ejection become unsmooth due to the clogging of cells, cell suspension was immediately removed from and recharged in the nozzle.

Results and discussion

Transport efficiencies of silica particles, yeast cells, and K562 cells in the conventional sample introduction system

Fig. 2 shows the transport efficiencies of SiO$_2$ particles, yeast cells, and K562 cells introduced into ICP-MS through the pneumatic nebulizer and the total consumption spray chamber of the conventional sample introduction system. The transport efficiencies are 66%, 5%, and 13% for 200 nm, 10 µm, and 20 µm SiO$_2$ particles, respectively. Although the cause is unclear, the transport efficiency of 20 µm SiO$_2$ particles is higher than that of 10 µm SiO$_2$ particles. If we ignore this unexpected result, the transport efficiency is considered to decrease as the particle size increases from nano to micrometer order. Despite the use of the total consumption spray chamber, efficient transport of large particles is hampered owing to the deposition of the particles onto the glass apparatus, such as the spray chamber and the ICP torch, during transport. For yeast cells measuring approximately 2 µm in diameter,[9] the transport efficiency is approximately 13%, which is a reasonable value compared with the transport efficiency of SiO$_2$ particles. Hence, the transport efficiency is mainly affected by particle/cell size rather than density or chemical composition. In contrast, the transport efficiency of approximately 20 µm-diameter K562 cells is around
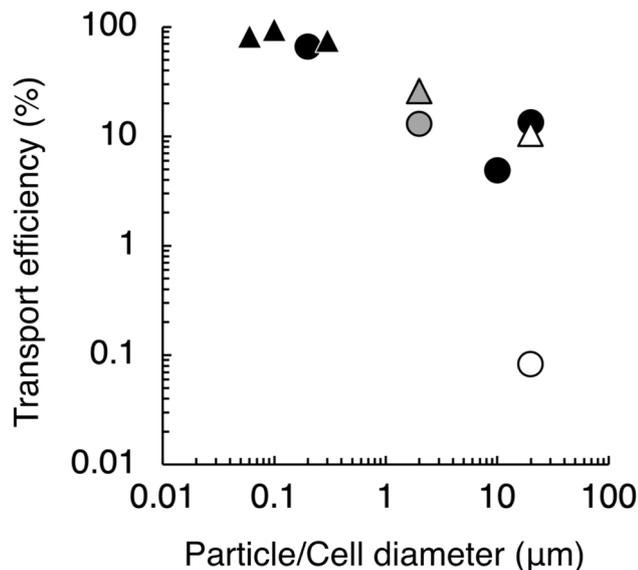
This journal is © The Royal Society of Chemistry 2025

J. Anal. At. Spectrom., 2025, **40**, 216–225 | **219**

Fig. 2 Transport efficiencies of SiO₂, Ag, and TiO₂ particles, yeast cells, and K562 cells. Black circle: SiO₂ particle, gray circle: yeast cell, white circle: K562 cell using the conventional sample introduction system for scICP-MS. Black triangle: Ag and TiO₂ nanoparticle, gray triangle: yeast cell, white triangle: K562 cell using μDG-ICP-MS. Data represent the average values of three repeated measurements. Error bars (SD) are included in each symbol.

0.1% and is significantly lower than that of same-sized SiO_2 particles. Unlike yeast cells, K562 cells have no cell wall and are therefore physically fragile. We have reported approximately

10% transport efficiency of rat red blood cells measuring around 5 μm in diameter,[9] although red blood cells do not have a cell wall. Therefore, we speculate that the larger the cell size, the greater the shear stress induced by the nebulization gas flow, which results in damage to cells.

Microscopy observation of K562 cells collected from pneumatic nebulizer

Fig. 3 illustrates microscopy images of cells collected from a nebulizer or a μDG. We observed cell damage by using two types of staining dyes (Fig. 3b and c). The number of undamaged cells collected from the nebulizer gradually decreased with increasing carrier gas flow rate. Moreover, numerous cell fragments stained with crystal violet were observed after nebulization at a high gas flow rate (Fig. 3c). These results indicate that K562 cells were damaged by nebulization with the pneumatic nebulizer. On the other hand, the structure of cells in droplets collected from the μDG was preserved, suggesting that the nondestructive introduction of mammalian cells is accomplished by droplet generation. Cell density increased for the cell suspension collected from the μDG. Because K562 cells tended to settle at the μDG tip, the cells concentrated inside the μDG nozzle. The results indicate that μDG improves the transport efficiency of cultured mammalian cells that are difficult to introduce by a nebulizer system.

Quantitative elemental analysis of ions in microdroplets

Fig. S1† shows the calibration curves of five essential elements obtained from differently sized microdroplets. The diameters of
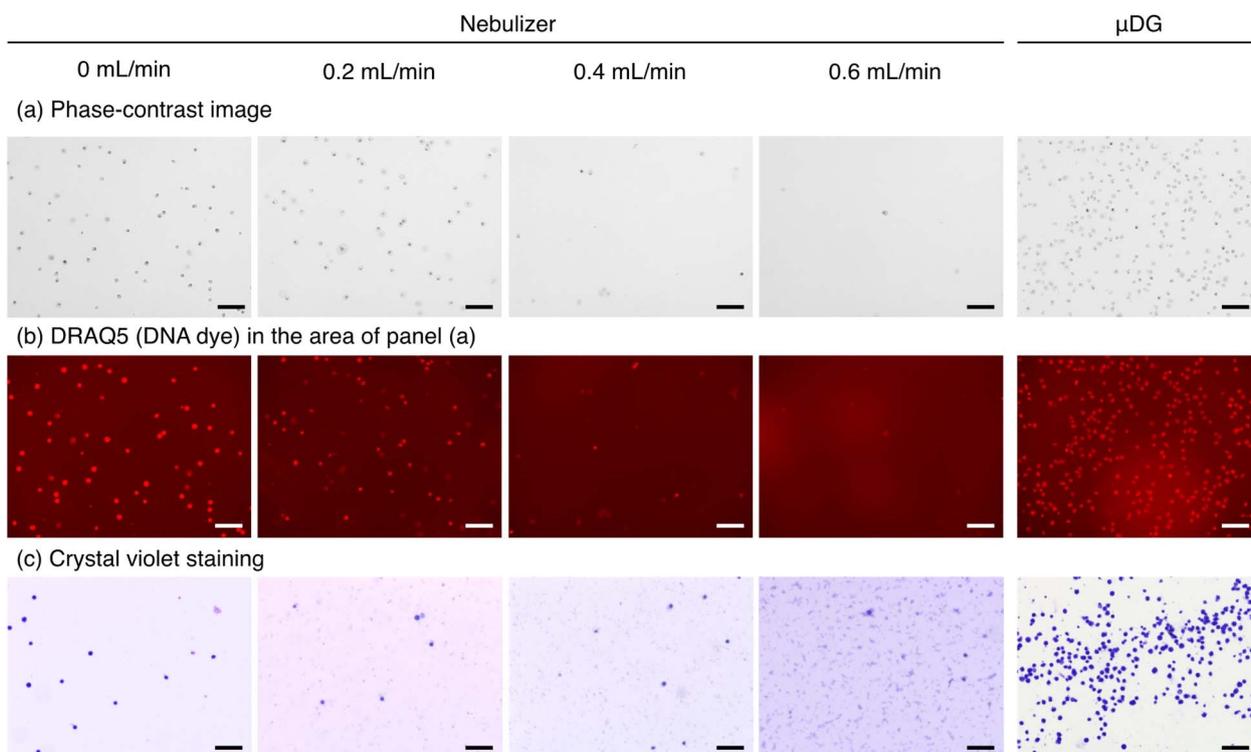

Fig. 3 Microscopy images of K562 cells collected from a pneumatic nebulizer or a μDG. (a) Phase-contrast images of unstained cells. (b) Fluorescence images of DRAQ5-stained cells. (c) Phase-contrast images of crystal violet-stained cells. Scale bars represent 150 μm.

220 | *J. Anal. At. Spectrom.*, 2025, **40**, 216–225
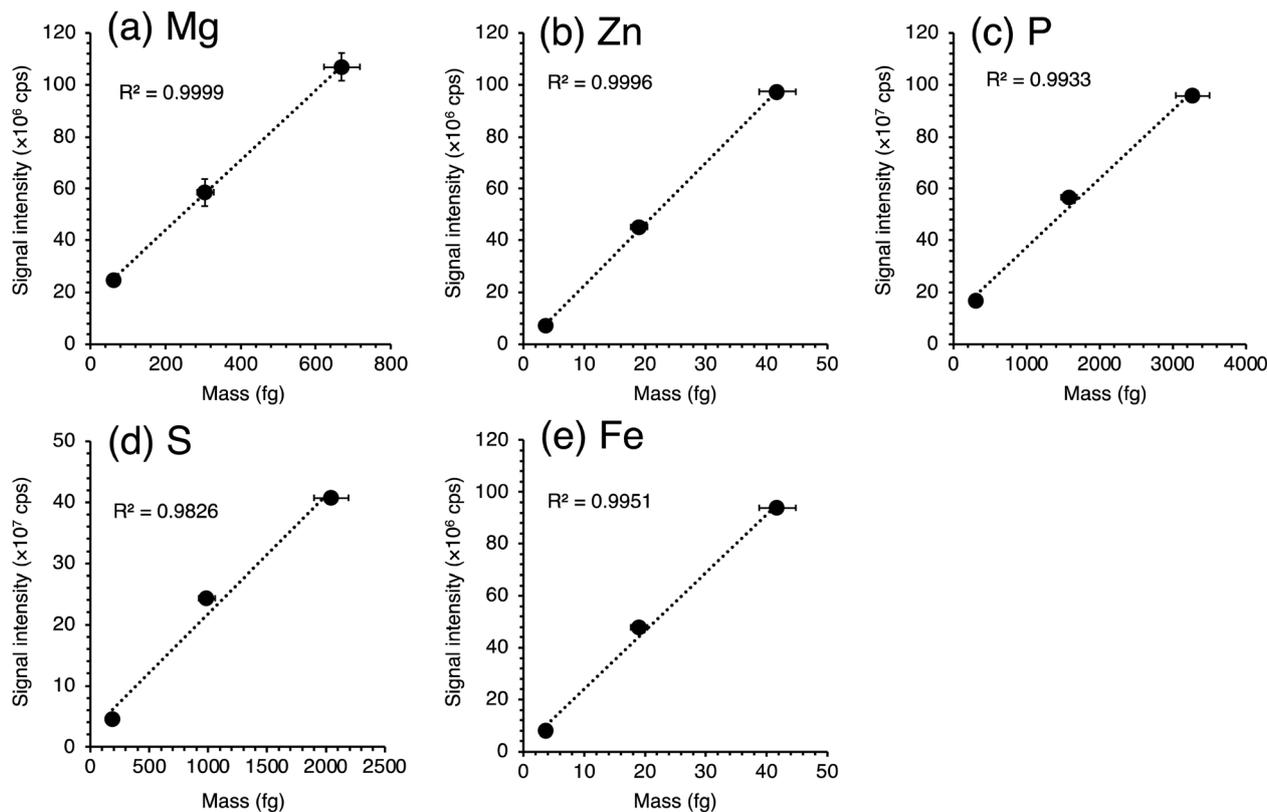
This journal is © The Royal Society of Chemistry 2025

Fig. 4 Calibration curves of five essential elements obtained from microdroplets of ionic standard solutions for K562. (a) Mg, (b) Zn, (c) P, (d) S, and (e) Fe.

droplets generated by three different types of μDGs are 37, 45, and 60 μm, which correspond to the droplet volumes of 27, 48, and 113 pL, respectively (Fig. S2†). When the same ionic standard solution is used, the masses of elements in a droplet are proportional to the droplet volume. Hence, the signal intensity of each droplet shows a linear relationship with its droplet volume (Fig. S1†). If the ionization of elements in large droplets (e.g., 60 μm) is suppressed, a non-linear regression curve would be obtained. However, we obtained a high linearity of the signals with respect to droplet volume, indicating that efficient ionization of elements even from large microdroplets was possible without the use of a heating device or a membrane desolvator. Fig. 4 shows the calibration curves of five essential elements obtained from the microdroplets of a series of ionic

standard solutions with different concentrations generated by a μDG having the smallest nozzle (IJHB30). High linearity of signals was obtained for the five elements. Therefore, we determined the elemental contents with the sensitivity factor, namely, the slope of the calibration curve for each element. The y-intercepts of the calibration curves for P, S, and Fe deviated from 0 cps owing to mass spectrometric interferences (e.g., $^1H^{14}N^{16}O_2^+$ for $^{31}P^{16}O^+$; $^{16}O_3^+$ for $^{32}S^{16}O^+$; and $^{40}Ar^{16}O^+$ for $^{56}Fe^+$). Hence, we measured multiple standard solutions, and the y-intercept was also considered in the calculation of elemental mass in yeast cells and K562 cells.

Correction of instrumental sensitivity drift was verified using the standard solution containing Mg, Zn, P, S, and Fe ions. The signal intensities from the droplets of ionic solution were
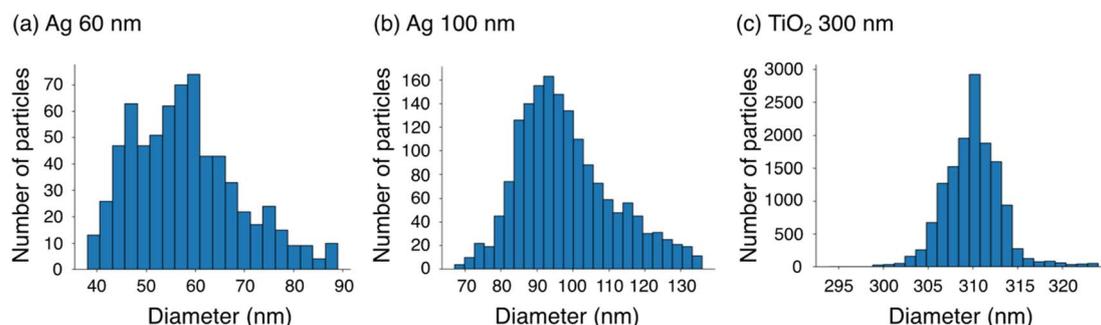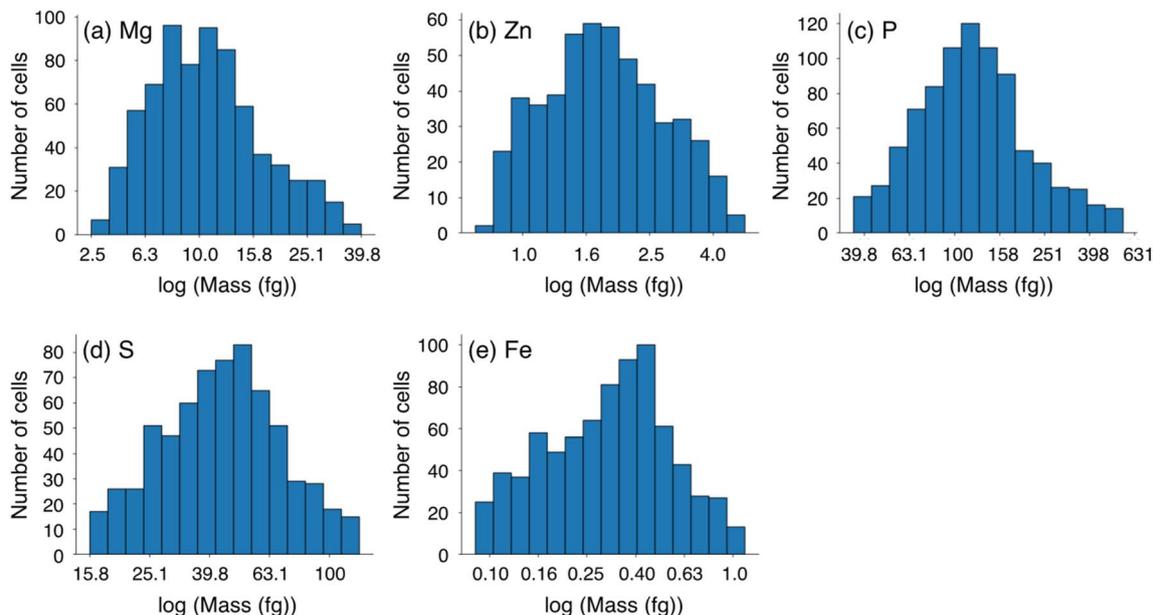

Fig. 5 Size distributions of nanoparticles obtained by μDG-ICP-MS. (a) Ag 60 nm, (b) Ag 100 nm, and (c) TiO$_2$ 300 nm.

This journal is © The Royal Society of Chemistry 2025

Table 2 Ag and TiO$_2$ particle sizes and transport efficiencies determined by μDG-ICP-MS

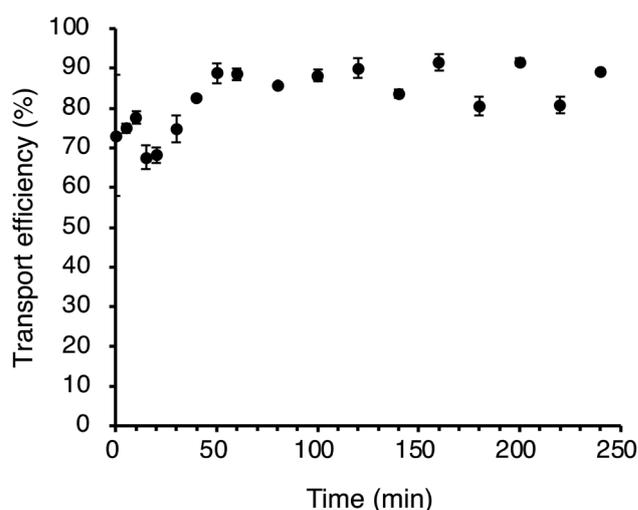|	Ag 60 nm	Ag 100 nm	TiO$_2$ 300 nm
Measured value in this study, nm	58.1 ± 10.9	97.9 ± 13.3	304.7 ± 61.7
Manufacturer's certified value, nm	60.0 ± 8	100 ± 8	305
Transport efficiency, %	82.3 ± 7.7	94.6 ± 1.0	75.0 ± 1.2

Fig. 6 Mass distributions of five essential elements in single yeast cells obtained by μDG-ICP-MS.

changed by altering the ICP-MS parameters. However, when the signals were corrected based on the signals of nebulized standard solution, the deviations became lower (Fig. S3†). Since actual instrumental sensitivity drift can be more slight comparing with the changes in this validation experiment, we concluded that correction of instrumental sensitivity works properly.

Validation of quantitative elemental analysis of a single nanoparticle or cell by μDG-ICP-MS

We validated the quantification by μDG-ICP-MS using Ag and TiO$_2$ nanoparticles. Transient signals of Ag and Ti were detected, as shown in Fig. S4.† The size distributions of the nanoparticles analyzed by μDG-ICP-MS are shown in Fig. 5. A single normal distribution approximates the size distributions to determine the average particles size and standard deviation. The average nanoparticle sizes are 58.1 ± 10.9 nm for 60 nm Ag, 97.9 ± 13.3 nm for 100 nm Ag, and 304.7 ± 61.7 nm for 300 nm TiO$_2$, consistent with the certified values provided by the manufacturers (Table 2, 60 ± 8 nm for 60 nm Ag, 100 ± 8 nm for 100 nm Ag, and 305 nm for 300 nm TiO$_2$). Several signals with approximately double intensity were detected in the signal profiles of time-resolved analysis (Fig. S4†). These can be derived from the simultaneous detection of two nanoparticles. Therefore, we analyzed the particle size distribution after rejecting signals with double heights.

In addition to nanoparticles, yeast cells of which elemental contents were previously reported were used for validation. Transient signals were detected for Mg, Zn, P, S, and Fe (Fig. S5†), and the mass distributions of these elements were obtained (Fig. 6). The average mass of each element in single yeast cells is 12.4 ± 0.3 fg for Mg, 2.04 ± 0.07 fg for Zn, 140 ± 5 fg for P, 49.0 ± 0.7 fg for S, and 0.358 ± 0.006 fg for Fe. The

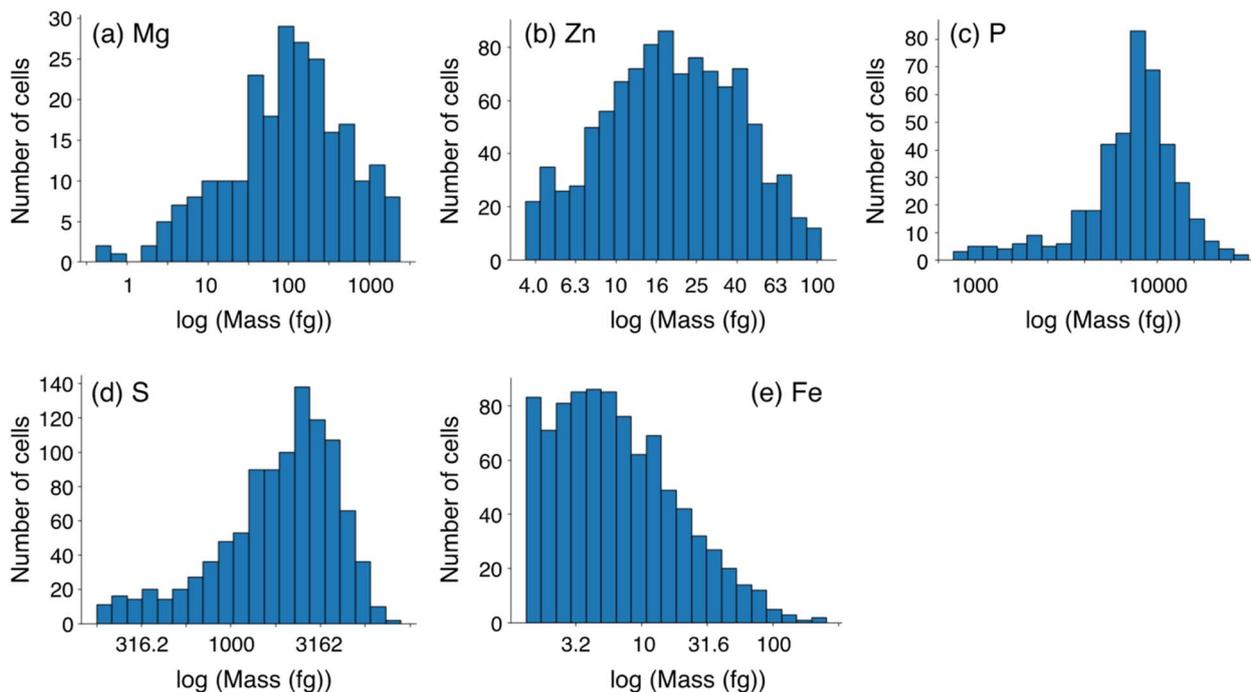**Fig. 7** Transport efficiency of TiO$_2$ nanoparticles introduced by using μDG over 4 h.

Fig. 8 Mass distributions of five essential elements in single K562 cells obtained by µDG–ICP-MS.

resulting mass values agree with previously reported values for acid-digested yeast samples. The relative mass differences between the single-cell analysis and the solution nebulization ICP-MS analysis are large for trace elements such as Zn and Fe. In this study, we corrected instrumental sensitivity drift by utilizing the signal intensities of ionic standard solutions nebulized from a concentric nebulizer (Fig. 1). As shown in Fig. S3,† changes in instrumental sensitivity were successfully corrected. When no correction was applied, the calculated masses of elements for the yeast cells greatly deviated from the reference values. This implies that analysis in the dry plasma condition is susceptible to instrumental sensitivity drift. For Zn and Fe, changes in instrumental sensitivity and/or the polyatomic interference production rate seem to be too large to be compensated by the correction.

The transport efficiencies of the nanoparticles and the yeast cells are 82.3% for 60 nm Ag, 94.6% for 100 nm Ag, 75.0% for 300 nm TiO_2, and 25.8% for yeast cells. Transport efficiencies of nanoparticles and yeast were comparable to or higher than those obtained in the conventional scICP-MS analysis using nebulizer system (Fig. 2). As mentioned above, the lower

transport efficiency of yeast cells than those of Ag and TiO_2 nanoparticles can be attributed to the deposition of the cells in the T-shaped glass plumbing and the ICP torch during transportation. In addition, the transport efficiency of TiO_2 nanoparticle was almost constant over 4 h (Fig. 7), suggesting sample introduction at a constant efficiency is possible. From the results obtained, we conclude that the present quantification analysis by µDG-ICP-MS can precisely determine elemental contents in single nanoparticles and cells.

Elemental analysis of single K562 cells by µDG-ICP-MS

Finally, we measured the five essential elements in single K562 cells by µDG-ICP-MS developed in this study. Transient signals were efficiently detected for Mg, Zn, P, S, and Fe (Fig. S6†). The mass distributions are shown in Fig. 8. The average mass values of the five elements in single K562 cells are 270 ± 100 fg for Mg, 23.0 ± 2.0 fg for Zn, 7684 ± 675 fg for P, 2136 ± 165 fg for S, and 14.4 ± 1.2 fg for Fe (Table 3). These data correspond well with the intracellular elemental contents obtained by bulk concentration analysis after acid digestion, namely, 343 ± 40 fg for Mg, 26.1 ± 3.4 fg for Zn, 5167 ± 443 fg for P, 1668 ± 122 fg for S, and

Table 3 Average mass values of five essential elements and transport efficiencies of single-cell samples

		Mg	Zn	P	S	Fe	Transport efficiency
Yeast	Single-cell ICP-MS with µDG	12.4 ± 0.3	2.04 ± 0.07	140 ± 5	49.0 ± 0.7	0.358 ± 0.006	25.8 ± 8.2
	Solution nebulization ICP-MS[a]	11.1 ± 0.2	1.26 ± 0.05	114 ± 4	45.4 ± 1.0	0.542 ± 0.009	—
K562	Single-cell ICP-MS with µDG	270 ± 100	23.0 ± 2.0	7684 ± 675	2136 ± 165	14.4 ± 1.2	10.5 ± 4.6
	Solution nebulization ICP-MS	343 ± 40	26.1 ± 3.4	5167 ± 443	1668 ± 122	20.2 ± 2.3	—
		fg per cell	fg per cell	fg per cell	fg per cell	fg per cell	%

[a] Data from ref. 9 (Tanaka et al., 2020). Uncertainties represent standard deviations calculated from three repeated analyses.

This journal is © The Royal Society of Chemistry 2025

J. Anal. At. Spectrom., 2025, 40, 216–225 | 223

20.2 ± 2.3 fg for Fe. For P and S contents, the values obtained by scICP-MS with μDG was slightly higher than those obtained by bulk concentration analysis. Some isobaric interferences derived from organic components of the cells (e.g., $^1H^{14}N^{16}O_2^+$ for $^{31}P^{16}O^+$; $^{31}P^1H^{16}O$ and $^{+16}O_3^+$ for $^{32}S^{16}O^+$) could not be completely removed even under the use of collision/reaction cell. However, because chemical fixation process caused significant loss of intracellular elements, especially for P, S, and Fe (Fig. S7†), we confirmed the advantage of μDG for the analysis of unfixed mammalian cells.

Furthermore, the transport efficiency of K562 cells is 10.5%, which is significantly higher than that obtained using a pneumatic nebulizer (Fig. 2). From these results, we conclude that the present quantification analysis by μDG-ICP-MS can precisely determine the elemental contents in single mammalian cells with high-throughput sample introduction.

Conclusion

We revealed that the conventional sample introduction system of ICP-MS prevented the efficient introduction of human chronic myelogenous leukemia K562 cells owing to cell damage. To overcome this problem, we installed a μDG into the sample introduction system for fast time-resolved ICP-MS analysis. Quantification was performed by creating calibration curves of elements in microdroplets of ionic standard solutions generated by the μDG. We demonstrated that the mass values of elements in nanoparticles and yeast cells were accurately determined by the quantification protocol established herein. Because μDG was capable of the nondestructive introduction of K562 cells, the transport efficiency of K562 cells was dramatically improved compared with that obtained by analysis using a pneumatic nebulizer. Furthermore, the measured elemental contents in K562 cells were consistent with the results of bulk concentration analysis after acid digestion. We confirmed that the μDG-ICP-MS method is a powerful approach for the elemental analysis of cultured mammalian cells at the single-cell level.

Data availability

The authors confirm that the data supporting the findings of this study are available within the article and its ESI.†

Conflicts of interest

The authors declare no conflict of interest.

Acknowledgements

References

1 B. Gomez-Gomez, M. Corte-Rodríguez, M. T. Perez-Corona, J. Bettmer, M. Montes-Bayón and Y. Madrid, *Anal. Chim. Acta*, 2020, **1128**, 116–128.

2 Y.-k. Tanaka, S. Shimazaki, Y. Fukumoto and Y. Ogra, *Anal. Chem.*, 2022, **94**, 7952–7959.

3 Y. Liang, Q. Liu, Y. Zhou, S. Chen, L. Yang, M. Zhu and Q. Wang, *Anal. Chem.*, 2019, **91**, 8341–8349.

4 L. Xu, A. Sigler, A. Chernatynskaya, L. Rasmussen, J. Lu, E. Sahle-Demessie, D. Westenberg, H. Yang and H. Shi, *Anal. Bioanal. Chem.*, 2024, **416**, 419–430.

5 A. S. Groombridge, S. Miyashita, S. Fujii, K. Nagasawa, T. Okahashi, M. Ohata, T. Umemura, A. Takatsu, K. Inagaki and K. Chiba, *Anal. Sci.*, 2013, **29**, 597–603.

6 K. Shigeta, G. Koellensperger, E. Rampler, H. Traub, L. Rottmann, U. Panne, A. Okino and N. Jakubowski, *J. Anal. At. Spectrom.*, 2013, **28**, 637–645.

7 Z. Liu, A. Xue, H. Chen and S. Li, *Appl. Microbiol. Biotechnol.*, 2019, **103**, 1475–1483.

8 R. Álvarez-Fernández García, M. Corte-Rodríguez, M. Macke, K. L. LeBlanc, Z. Mester, M. Montes-Bayón and J. Bettmer, *Analyst*, 2020, **145**, 1457–1465.

9 Y. K. Tanaka, R. Iida, S. Takada, T. Kubota, M. Yamanaka, N. Sugiyama, Y. Abdelnour and Y. Ogra, *Chembiochem*, 2020, **21**, 3266–3272.

10 X. Shen, H. Zhang, X. He, H. Shi, C. Stephan, H. Jiang, C. Wan and T. Eichholz, *Anal. Bioanal. Chem.*, 2019, **411**, 5531–5543.

11 E. Mavrakis, L. Mavroudakis, N. Lydakis-Simantiris and S. A. Pergantis, *Anal. Chem.*, 2019, **91**, 9590–9598.

12 M. v. d. Au, M. Schwinn, K. Kuhlmeier, C. Büchel and B. Meermann, *Anal. Chim. Acta*, 2019, **1077**, 87–94.

13 R. Gonzalez de Vega, S. Goyen, T. E. Lockwood, P. A. Doble, E. F. Camp and D. Clases, *Anal. Chim. Acta*, 2021, **1174**, 338737.

14 J. Shi, X. Ji, Q. Wu, H. Liu, G. Qu, Y. Yin, L. Hu and G. Jiang, *Anal. Chem.*, 2020, **92**, 622–627.

15 H. Wang, B. Chen, M. He and B. Hu, *Anal. Chem.*, 2017, **89**, 4931–4938.

16 H. Wang, B. Wang, M. Wang, L. Zheng, H. Chen, Z. Chai, Y. Zhao and W. Feng, *Analyst*, 2015, **140**, 523–531.

17 H. Wang, M. Wang, B. Wang, L. Zheng, H. Chen, Z. Chai and W. Feng, *Anal. Bioanal. Chem.*, 2017, **409**, 1415–1423.

18 Y. Cao, J. Feng, L. Tang, C. Yu, G. Mo and B. Deng, *Talanta*, 2020, **206**, 120174.

19 M. Corte-Rodriguez, R. Alvarez-Fernandez Garcia, P. Garcia-Cancela, M. Montes-Bayón, J. Bettmer and D. J. Kutscher, *Spectroscopy Supplements*, 2020, **18**, 6–10.

20 Y. Zhou, H. Wang, E. Tse, H. Li and H. Sun, *Anal. Chem.*, 2018, **90**, 10465–10471.

21 P. Chen, M. He, B. Chen and B. Hu, *Ecotoxicol. Environ. Saf.*, 2020, **205**, 111110.

22 C. Wu, X. Wei, X. Men, X. Zhang, Y.-L. Yu, Z.-R. Xu, M.-L. Chen and J.-H. Wang, *Anal. Chem.*, 2021, **93**, 8203–8209.

224 | *J. Anal. At. Spectrom.*, 2025, **40**, 216–225

This journal is © The Royal Society of Chemistry 2025

23 A. Galé, L. Hofmann, N. Lüdi, M. N. Hungerbühler, C. Kempf, J. T. Heverhagen, H. von Tengg-Kobligk, P. Broekmann and N. Ruprecht, *Int. J. Mol. Sci.*, 2021, **22**, 9468.

24 Y. Zhou, Z. Chen, J. Zeng, J. Zhang, D. Yu, B. Zhang, X. Yan, L. Yang and Q. Wang, *Anal. Chem.*, 2020, **92**, 5286–5293.

25 Z. Chen, B. Chen, M. He and B. Hu, *Anal. Chem.*, 2022, **94**, 6649–6656.

26 X. Zhang, X. Wei, X. Men, Z. Jiang, W.-Q. Ye, M.-L. Chen, T. Yang, Z.-R. Xu and J.-H. Wang, *Anal. Chem.*, 2020, **92**, 6604–6612.

27 X. Wei, X. Zhang, R. Guo, M.-L. Chen, T. Yang, Z.-R. Xu and J.-H. Wang, *Anal. Chem.*, 2019, **91**, 15826–15832.

28 L. N. Zheng, M. Wang, L. C. Zhao, B. Y. Sun, B. Wang, H. Q. Chen, Y. L. Zhao, Z. F. Chai and W. Y. Feng, *Anal. Bioanal. Chem.*, 2015, **407**, 2383–2391.

29 C. Wu, X. Men, M. Liu, Y. Wei, X. Wei, Y.-L. Yu, Z.-R. Xu, M.-L. Chen and J.-H. Wang, *Anal. Chem.*, 2023, **95**, 13297–13304.

30 J. Wang, X. Wei, C.-X. Wu, X. Zhang, Y.-J. Wei, J.-H. Liu, Y. Wang, M.-L. Chen and J.-H. Wang, *Anal. Chem.*, 2023, **95**, 16176–16184.

31 L. Gutierrez-Romero, E. Blanco-González and M. Montes-Bayón, *Anal. Chem.*, 2023, **95**, 11874–11878.

32 P. E. Verboket, O. Borovinskaya, N. Meyer, D. Günther and P. S. Dittrich, *Anal. Chem.*, 2014, **86**, 6012–6018.

33 K. Shigeta, H. Traub, U. Panne, A. Okino, L. Rottmann and N. Jakubowski, *J. Anal. At. Spectrom.*, 2013, **28**, 646–656.

34 T. Vonderach and D. Günther, *J. Anal. At. Spectrom.*, 2021, **36**, 2617–2630.

35 J. Koch, L. Flamigni, S. Gschwind, S. Allner, H. Longerich and D. Günther, *J. Anal. At. Spectrom.*, 2013, **28**, 1707–1717.

36 D. Rosenkranz, F. L. Kriegel, E. Mavrakis, S. A. Pergantis, P. Reichardt, J. Tentschert, N. Jakubowski, P. Laux, U. Panne and A. Luch, *Anal. Chim. Acta*, 2020, **1099**, 16–25.

37 J. Kocic, D. Günther and B. Hattendorf, *J. Anal. At. Spectrom.*, 2021, **36**, 233–242.

This journal is © The Royal Society of Chemistry 2025

J. Anal. At. Spectrom., 2025, **40**, 216–225 | **225**